ACS APPLIED MATERIALS & INTERFACES

Research Article

www.acsami.org

Codoping-Induced, Rhombus-Shaped Co_3O_4 Nanosheets as an Active Electrode Material for Oxygen Evolution

Xiaoli Zhang,*[,†] Jinbao Zhang,[‡] and Kai Wang*[,†]

[†]Department of Electrical & Electronic Engineering, South University of Science and Technology of China, Shenzhen, 518055, China
Shenzhen Key Laboratory of Third Generation Semiconductor Devices (SUSTC), Shenzhen, 518055, China

[‡]Physical Chemistry, Centre of Molecular Devices, Department of Chemistry Ångström Laboratory, Uppsala University, Uppsala, Sweden SE-75120

Supporting Information

ABSTRACT: Nanostructured Co_3O_4 doped with Zn^{2+}, Ni^{2+}, and both were directly grown on an ITO substrate by an easily available hydrothermal method. The doped Co_3O_4 showed a unique structural morphology evolution upon controlling the doping elements and the doping ratio of the cations. For the codoped samples, the novel rhombus-shaped Co_3O_4 nanosheets doped with Zn^{2+} and Ni^{2+} (concentration ratio of 1:2) exhibited the optimal electrocatalytic performance. The sample showed a current density of 165 mA cm^{-2} at 1.75 V, approximately 1.6 and 4 times higher than that of samples doped with Zn^{2+} and Ni^{2+} at a concentration ratio of 1:1 and 1:3. The unique architecture and its corresponding modified physical properties, such as high active-site density created by codoping, large structural porosity, and high roughness, are together responsible to its superior performance. For codoped Co_3O_4 nanostructures, Zn^{2+} facilitates the creation of Co cations in their high oxidation state as active centers, while Ni^{2+} contributed to the new active sites with lower activation energy. The synergistic effect of Zn^{2+} and Ni^{2+} doping can explain the improved physicochemical properties of codoped Co_3O_4 nanostructures.

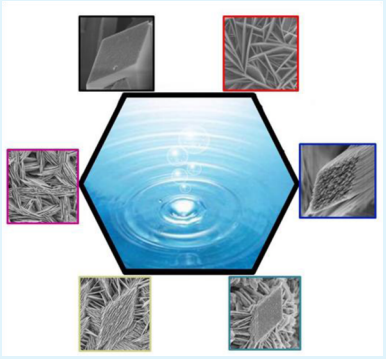

KEYWORDS: *water splitting, oxygen evolution reaction, electrocatalysis, codoped Co_3O_4, nanostructures*

1. INTRODUCTION

Electrochemical systems play key roles in a number of efficient and environment-friendly technologies for energy conversion and storage, such as supercapacitors, lithium ion batteries, and water-splitting devices.[1−3] The accompanying energy conversion in an electrochemical reaction is a straightforward and clean process that does not generate any environmental pollution. In particular, the oxygen evolution reaction (OER) in the water-splitting system, as one of the most promising electrochemical techniques to provide clean fuel, has been widely investigated and developed in recent years.[4−8] Herein, a great deal of effort has been made to look for highly effective OER electrocatalysts for the efficient water oxidation in terms of low overpotential and low cost.[4] Besides, the utilization of an OER electrocatalyst with long-term stability upon prolonged exposure to oxidizing conditions is also essential for the electrocatalysis. The widely studied catalysts based on the metal oxides RuO_2 and IrO_2 are commonly considered as highly efficient OER catalysts; however, their earthly scarcity and high cost undoubtedly limit their large-scale utilization.[5,6] In this respect, the development of new alternatives of OER electrocatalysts based on inexpensive transition-metal elements has attracted great attention in this community.[7,8] Particularly, earth-abundant cobalt-based catalyst and its substituted cobaltites have demonstrated their good catalytic activity and corrosion stability and been recognized as some of the most promising electroactive materials for the electrochemical OER.[9−11]

Generally, the electrochemical reaction and the simultaneous charge transfer in the OER process occur at the interfaces. Therefore, the structural morphology of the employed electrode material could significantly affect the kinetics of the corresponding electrochemical reaction in the cells.[12,13] Previous studies have shown that cobalt-based spinel oxides for OER are generally obtained in the form of thin films or particle agglomerates physically loaded on the conductive substrates.[14,15] However, in these architectures, the imperfect electrical contact with a large resistance between the active electrode materials and the current collector greatly impedes the effective charge transfer at the interfaces. Recently, cobalt-based active components with well-aligned nanostructures have been successfully grown on conductive substrates, showing high electrical conductivity and low diffusion resistance.[13,16] The approach of the direct growth of nanostructures on the conductive substrate could not only avoid the use of the polymer binder or conductive additives but also substantially reduce the dead volume in the electrode materials. In this paper, nanohierarchical Co_3O_4 was directly prepared on

Received: June 11, 2015
Accepted: September 18, 2015
Published: September 18, 2015

DOI: 10.1021/acsami.5b05149
ACS Appl. Mater. Interfaces 2015, 7, 21745−21750

indium−tin oxide (ITO) substrate by an easily available hydrothermal method. Moreover, the evolution of the novel morphology of nano-Co_3O_4 was observed by controlling the doping levels of Zn^{2+} and Ni^{2+} dopants, and subsequently, a highly efficient OER was achieved by using the doped electrode material. In addition, the physicochemical effects of the Zn^{2+} and Ni^{2+} dopants are discussed.

2. RESULTS AND DISCUSSION

Characterization and Results. Nanostructured Co_3O_4 doped with Zn^{2+}, Ni^{2+}, and both, denoted as ZCO, NCO, and ZNCO, respectively, were grown directly on the ITO substrate in a mixed aqueous solution containing $Co(NO_3)_2$, $Zn(NO_3)_2$, and $Ni(NO_3)_2$ precursors via ammonia-evaporation-induced growth.[17] As shown in the scanning electron microscope (SEM) images in Figure 1, Co_3O_4 nanorods with

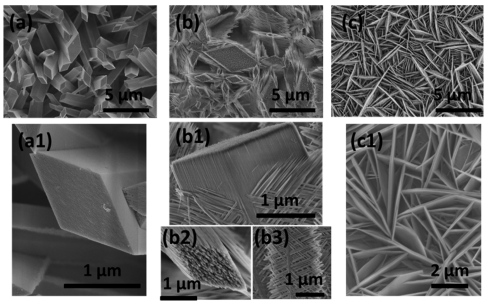

Figure 1. SEM images of doped Co_3O_4 nanostructures grown on ITO conductive substrate: (a, a1) Co_3O_4, (b, b1, b2, b3) ZCO, and (c, c1) NCO.

rhombic cross section were densely grown on the entire surface of the ITO substrate, with a width and length of 1 and 10 μm, respectively. After doping with Zn^{2+} and Ni^{2+}, the surface morphology was evolved into nanoarrays and nanoplates (Figure 1b,c), respectively. Though ZCO nanoarrays were formed with nanowires on the top and sides, they also roughly followed the rhombic feature of spinel Co_3O_4 nanorods.

To further investigate the effects of dopants, Zn^{2+} and Ni^{2+} were codoped in Co_3O_4 with doping levels of 1:1, 1:2, and 1:3 (denoted as ZNCO-1, ZNCO-2, and ZNCO-3, respectively). A surprising morphology evolution emerged in the final products, as shown in Figure 2. After Zn^{2+} and Ni^{2+} codoping, the morphologies of ZNCO-1 exhibited rhombic columns consisting of crowded sheets. Uniform nanosheets ranked as rhombus were observed as the doping ratio increased to 1:2

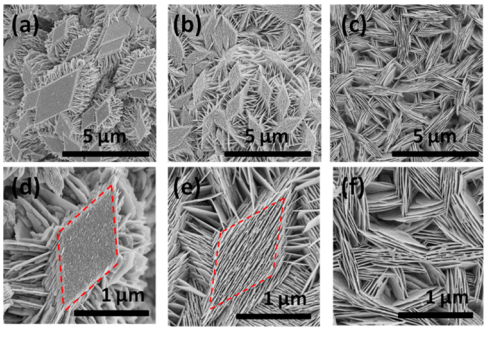

Figure 2. SEM images of doped Co_3O_4 nanostructures grown on ITO conductive substrate: (a, d) ZNCO-1, (b, e) ZNCO-2, and (c, f) ZNCO-3.

(Figure 2b). This is the first report that the doped Co_3O_4 nanosheets orderly arranged in rhombic shape. However, further Ni^{2+} doping resulted in a remarkable morphological transformation from hierarchical arrays to random nanoplates (Figure 2c). Such an amazing morphological difference highlights the importance of the doping elements and the doping levels. Particularly, Zn^{2+} doping promotes the morphological memory of the original rhombic-shaped Co_3O_4 structure, while Ni^{2+} doping creates a strong preference for the morphological evolution to NiO nanoplates.[17] For codoped samples, the diffraction peaks were maintained, as observed in the X-ray diffraction (XRD) patterns in Figure 3. The introduction of Ni^{2+} dopants resulted in a decreased *d*-spacing and (311) peak shift to a large angle, as indicated by the crystallographic properties of ZNCO samples [Table S-1, Supporting Information (SI)]. Actually, this result is ascribed to the presence of Ni^{3+} during doping, which could improve the electric conductivity of codoped samples, as will be discussed later.

The unique hierarchical nanostructures of ZNCO-2 provided a large specific surface area and high porosity, as indicated by transmission electron microscopy (TEM), as shown in Figure 4. The individual nanosheet was taken from a rhombus-shaped ZNCO-2 electrode. The nanosheet was porous with a rough surface, as commonly seen in oxides obtained from hydrate precursors.[18] The pores were believed to be generated in the calcination process because of CO_2 release.[18] The corresponding fast-Fourier transformation (FFT) patterns showed rings with several brighter dots, indicating their polycrystalline characteristics. This unique porous architecture ensured its long-term stability and provided highways for both fast ion diffusion and electron transfer in the Co_3O_4 network. From Brunauer−Emmett−Teller (BET) measurements, ZNCO-2 showed a relatively high specific surface area of 70.5 $m^2\ g^{-1}$ (Table S-1, SI), which is highly desirable for efficient electrochemical reactions at the interface between electrodes and electrolytic solution. The high-resolution TEM image provides detailed structural information about the grain size of the crystalline ZNCO-2 nanoparticles, being approximately 5−10 nm. The lattice fringes showed a lattice spacing of 0.23 nm, corresponding to the (222) planes of cubic ZNCO-2. The doping level was measured by means of energy dispersive spectrometry (EDS). The overall Zn/Ni ratio of the doped samples was found to decrease because of the introduction of Ni^{2+} (Table S-1, SI), while Co, Ni, and Zn elements were distributed uniformly in ZNCO-2 nanostructures, as confirmed by the element mapping results.

The as-synthesized Co_3O_4 nanostructures doped with different elements were directly employed as electrode materials in OER. The electrochemical experiments were carried out in a three-electrode glass cell in 1 M KOH aqueous solution. The linear-sweep measurement was employed to confirm the OER electrocatalytic activity of the different active materials, as shown in Figure 5. Apparently, Zn^{2+}- or Ni^{2+}-doped samples exhibited enhanced catalytic activity compared to undoped Co_3O_4 by considering the generated current at a given potential. For the codoped samples, ZNCO-2 and ZNCO-3 exhibited the high current densities of 165 and 105 mA cm^{-2} at 1.75 V, showing values approximately 4 and 3 times higher than that of ZNCO-1 (39 mA cm^{-2}), respectively.

Accordingly, the Tafel behavior could provide important information on the kinetic parameters and the probable changes of the OER mechanism. Tafel slopes of 62 and 65

DOI: 10.1021/acsami.5b05149
ACS Appl. Mater. Interfaces 2015, 7, 21745−21750

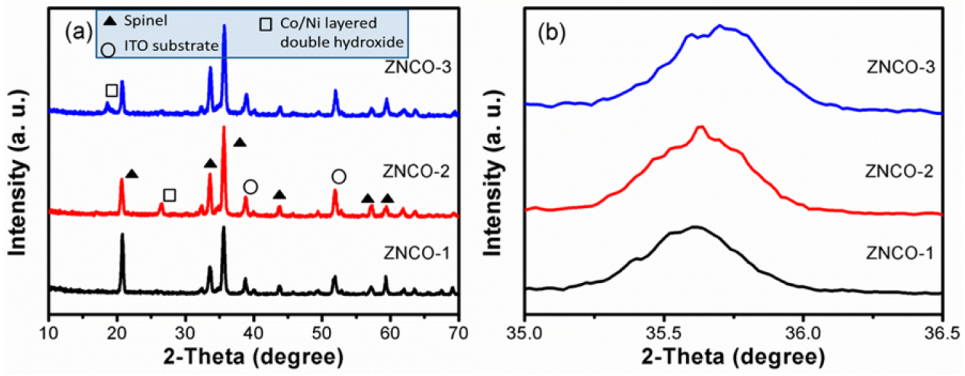

Figure 3. (a) XRD results of codoped samples: ZNCO-1, ZNCO-2, and ZNCO-3. (b) Comparison of the diffraction peak (311).

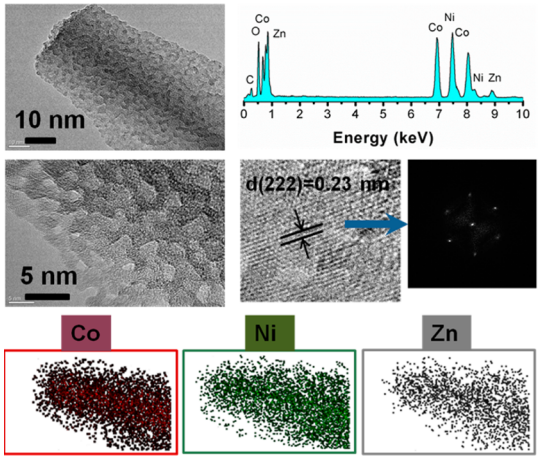

Figure 4. TEM images of ZNCO-2 with the associated EDX line profile and elements mapping (Co, Ni, Zn).

mV decade^{-1} were recorded for the ZNCO-2 and ZNCO-3 electrodes, respectively, demonstrating that the catalysts exhibited a similar rate-determining step (RDS) for the OER. The RDS and the Tafel slope depend on the adsorption strength of the intermediates on the active materials, while the corresponding adsorption strength was strongly determined by the physicochemical properties of the oxide electrodes.[19−21] Because of the formation of the intermediate product MOH (M is the active site) and the fact that the adsorbed intermediate as an unstable species could rearrange through the surface reaction, a pre-equilibrium mechanism has been widely recognized in previous studies.[15,22] Consequently, the variation of Tafel slopes could be explained by an OER mechanism involving a pre-equilibrium. Specifically, it could consist of a possible one-electron electrochemical step: MOH + $OH^- \rightarrow MO + H_2O + e^-$.[15] Therefore, except for the large specific surface area from the mesoporous structure, the enhanced performance of ZNCO-2 could also be attributed to the isomorphous replacement of Co^{2+} with Zn^{2+} and Ni^{2+}.[22]

Metal cations in high oxidation states have been proposed as active sites for OER catalysts based on the oxides of Mn, Ni, and Ir.[23−26] In support of this interpretation, cyclic voltammetry (CV) of different electrode materials in the

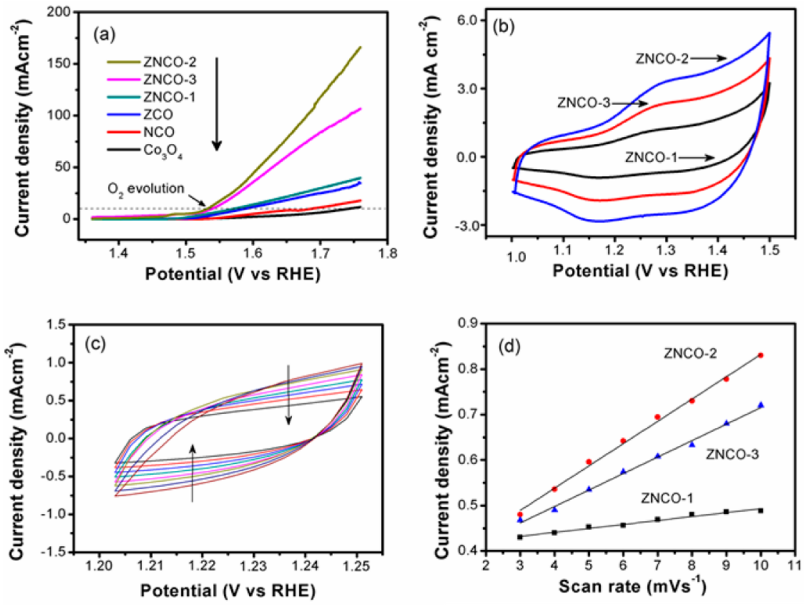

Figure 5. (a) State polarization curves recorded at a scan rate of 0.5 mV s^{-1}. (b) Cyclic voltammograms of codoped Co_3O_4 nanostructures (ZNCO-1, ZNCO-2, ZNCO-3). (c) Cyclic voltammograms of ZNCO-2 as a function of the scan rate, along the arrow direction: 10, 9, 8, 7, 6, 5, 4, and 3 mV s^{-1}. (d) Dependence of the capacitive current on the scan rate of ZNCO samples.

DOI: 10.1021/acsami.5b05149
ACS Appl. Mater. Interfaces 2015, 7, 21745−21750

electrolytic solution was carried out between 1.0 and 1.5 V at a scan rate of 5 mV s^{-1} (Figure 5b). A small anodic peak and a corresponding cathodic peak were observed for ZNCO-1 electrode, whereas ZNCO-2 and ZNCO-3 samples showed much stronger redox peaks. The anodic and cathodic peaks in CV patterns correspond to the formation of cobalt oxide phases with different oxidation states, and the pair of redox peaks can be assigned to the Co^{2+}/Co^{3+} or Co^{3+}/Co^{4+}. The CV patterns shows some variation from sample-to-sample and strongly depend on the morphology and surface properties of the active materials.[27,28] To illustrate the doping effects, the anodic peaks were used to quantify the redox characteristics of codoped samples. The area of the anodic peak of ZNCO-2 was approximately twice than that of ZNCO-1, indicating a significantly large active surface for the electrocatalytic oxygen evolution. Furthermore, the codoped samples ZNCO-2 and ZNCO-3 showed their increased number of active centers by considering of the number of active sites per unit surface area (Table S-1, SI). The number was derived from the voltammetric charge by integrating the anodic peak area. The roughness factor of the surface structure was also calculated on the basis of the double-layer capacitance of active electrodes in solution by assuming a standard value of 60 μF cm^{-2} for oxide surface, and ZNCO-2 shows a 7-fold increase in roughness factor than ZNCO-1 (Figure 5c,d).

Roles of Codoping on the Performance. X-ray photoelectron spectroscopy (XPS) provides information on the chemical states upon the variation in binding energy or chemical shifts of the photoelectron lines. As the Ni^{2+} doping amount increased, a negative shift of Co 2p was observed for ZNCO samples (Figure S-1, SI). The binding energy shift is a process of changing the ionic charge of the atom. It has been reported that the decrease in binding energy of Co 2p is due to the electron transfer between the hybrid structure, which enhances the catalytic properties.[7] Therefore, the increased Ni^{2+} doping may have the potential ability to change the ionic charge and lead to the fast energy transfer with a reduced binding energy. Furthermore, Ni^{2+} doping promotes the electronic conductivity of active materials, which was confirmed by electrochemical impedance spectroscopy (EIS) fitted by an equivalent circuit (Figure S-2, SI). The equivalent circuit consists of a constant-phase element (CPE), a charge-transfer resistance (R_{ct}), a pseudocapacitive element (C_p) in parallel, and an internal resistance (R_s). The ZNCO-2 and ZNCO-3 electrodes possessed smaller resistance, indicating a high charge-transfer rate between the electrolyte and the active material. This result agrees with CV and linear-sweep results. Thus, Ni^{2+} doping facilitates the sample to have a better utilization of electrons during the electrochemical process. The introduction of Ni^{3+} to the Co_3O_4 spinel lattice at octahedral sites was reported to increase the conductivity of samples up to 5 orders of magnitude.[29,30] Therefore, Ni doping of samples contributed to a high efficiency of the electrochemical reaction.

To explore the origin of the improved physicochemical properties of Co_3O_4 upon doping, a detailed discussion on how the metal cations and the active centers contribute to the improved performance of the codoped samples follows. (1) The incorporation of foreign Zn^{2+} into the Co_3O_4 lattice leads to a change in the chemical environment of Co ions. Zn^{2+} ions occupying tetrahedral sites increase the distance of the Co−O bonds, which enables the adsorption of the anions (OH^-) onto the Co cations and thus facilitates the transformation of Co^{3+}/Co^{4+} as follows: $CoOOH + OH^- \rightarrow CoO_2 + H_2O + e^-$.[14,31] The creation of Co^{4+} species as active centers contributed to the advanced OER activity. (2) The incorporation of Ni^{2+} into the structure produces more polarons in the material.[32] Ni doping also contributes to the high active surface area by creating new active sites with lower activation energy.[33] As the Ni doping level increased, a small negative shift of the anodic peak of ZNCO samples was observed, which could result from the Ni^{3+}/Ni^{4+} oxidation.[34] Therefore, the synergetic effect of Zn^{2+}-doping-induced Co^{3+}/Co^{4+} oxidation and Ni^{2+}-doping-induced Ni^{3+}/Ni^{4+} oxidation together enhanced the performance of the codoped ZNCO electrodes.

3. CONCLUSION

In summary, doped Co_3O_4 nanostructures showed unique structural morphology evolution by controlling the doping elements and the doping ratio of the cations. A novel rhombus-shaped Co_3O_4 nanosheet ZNCO-2 was successfully obtained under the doping ratio of 1:2 (Zn:Ni), and ZNCO-2 electrode exhibited the optimal electrocatalytic performance, with a higher anodic current for oxygen evolution than the active materials with other doping levels. The unique architecture and its corresponding modified physical properties, such as high active-site density created by codoping, large structural porosity, and high roughness, are together responsible to its superior electrocatalytic performance. Given the low cost and easy fabrication in a large area, the ZNCO-2 with rhombus-shaped nanostructures obtained by effective codoping holds a large potential as a highly promising electrocatalyst in the future. Inspired by the conclusions above, the research can also be extended to other cation-codoped (Cu^{2+}, Mn^{2+}, Li^+) Co_3O_4 nanostructures for catalyzing the oxygen evolution efficiently.

4. MATERIALS AND METHODS

Synthesis of Doped Co_3O_4 Nanostructures on ITO Substrate. All chemical were analytical grade, purchased from Aladdin Co., and used without further purification. In a typical synthesis, 0.1 M $Zn(NO_3)_2$ or 0.1 M $Ni(NO_3)_2$ was added into 50 mL of 0.4 M $Co(NO_3)_2$ aqueous solution with NH_4F and $CO(NH_2)_2$ as addictives at room temperature, respectively. The as-formed homogeneous solution was then transferred into a Teflon-lined stainless steel autoclave containing cleaned ITO substrate. The sealed autoclave was maintained at 100 °C for 8 h and allowed to cool to room temperature naturally. The substrate was washed several times with distilled water and then dried at room temperature. The as-grown nanostructures were annealed at 250 °C for 2 h before use and characterization. To address the effects of the Ni^{2+} dopant, the concentration variation of $Ni(NO_3)_2$ in the precursor was studied under some fixed reaction conditions, such as $Zn(NO_3)_2$ concentration (0.1 M), reaction temperature, and time. In detail, the $Ni(NO_3)_2$ concentration was increased to 0.2 and 0.3 M from 0.1 M. For the codoped samples with $Zn(NO_3)_2$ and $Ni(NO_3)_2$, a concentration ratio of 1:1, 1:2, or 1:3 was denoted as ZNCO-1, ZNCO-2, or ZNCO-3, respectively. For codoped samples, the growth process follows the same procedure, but there is just codeposition of $Zn(NO_3)_2$ and $Ni(NO_3)_2$ precursors at different ratios.

Characterization. XRD was performed on a Shimadzu XRD-6000 diffractometer with Cu Ka radiation (λ = 0.154 06 nm). The surface morphology of as-synthesized samples was monitored using a SEM system. The structure and composition of the products were characterized using a TEM system equipped with an EDS instrument. The BET surface of the catalysts was measured by N_2 absorption using the single-point method.

Electrochemical Measurements. Doped Co_3O_4 nanostructures grown on ITO substrate were directly used as anode for the electrochemical characterization. Electrochemical experiments were carried out in a three-electrode glass cell in 1 M KOH solution using a

DOI: 10.1021/acsami.5b05149
ACS Appl. Mater. Interfaces 2015, 7, 21745−21750

carbon counter electrode and an Hg/HgO reference electrode with CHI-660D to collect data. Steady-state OER polarization curves were obtained at a scan rate of 0.5 mV s^{-1}. For cyclic voltammograms, working electrodes were cycled 10 times before data were collected between 1.0 and 1.5 V at different scan rates.

■ ASSOCIATED CONTENT

Supporting Information

The Supporting Information is available free of charge on the ACS Publications website at DOI: 10.1021/acsami.5b05149.

typical XPS spectra of different samples (Figure S-1); a comparison of EIS measurements of ZNCO-1, ZNCO-2, and ZNCO-3 (Figure S-2); and physical and chemical properties for doped samples (Table S-1) (PDF)

■ AUTHOR INFORMATION

Corresponding Authors

*X.Z.: tel/fax, +86 755 88018181; e-mail, xlzhang@tju.edu.cn.
*K.W.: e-mail, wangk@sustc.edu.cn.

Notes

The authors declare no competing financial interest.

■ ACKNOWLEDGMENTS

This work was supported by National Natural Science Foundation of China (Grant No. 51402148), Guangdong High Tech Project (Grant No. 2014A010105005, No. 2014TQ01C494), Shenzhen Nanshan Innovation Project (Grant No. KC2014JSQN0011A), and SUSTC Foundation (Grant No. FRG-SUSTC1501A-48).

■ REFERENCES

(1) Tong, G.; Guan, J.; Zhang, Q. In Situ Generated Gas Bubble-directed Self-assembly: Synthesis, and Peculiar Magnetic and Electrochemical Properties of Vertically Aligned Arrays of High-density Co_3O_4 Nanotubes. *Adv. Funct. Mater.* **2013**, *23*, 2406−2414.

(2) Yuan, C.; Yang, L.; Hou, L.; Shen, L.; Zhang, X.; Lou, X. W. Growth of Ultrathin Mesoporous Co_3O_4 Nanosheet Arrays on Ni Foam for High-performance Electrochemical Capacitors. *Energy Environ. Sci.* **2012**, *5*, 7883−7887.

(3) Zhang, X.; Li, Y.; Zhao, J.; Wang, S.; Li, Y.; Dai, H.; Sun, X. Advanced Three-component ZnO/Ag/CdS Nanocomposite Photoanode for Photocatalytic Water Splitting. *J. Power Sources* **2014**, *269*, 466−472.

(4) Herrero, C.; Quaranta, A.; Leibl, W.; Rutherford, A. W.; Aukauloo, A. Artificial Photosynthetic Systems Using light and Water to Provide Electrons and Protons for The Synthesis of A Fuel. *Energy Environ. Sci.* **2011**, *4*, 2353−2365.

(5) Frame, F. A.; Townsend, T. K.; Chamousis, R. L.; Sabio, E. M.; Dittrich, T.; Browning, N. D.; Osterloh, F. E. Photocatalytic Water Oxidation With Nonsensitized IrO_2 Nanocrystals Under Visible and UV Light. *J. Am. Chem. Soc.* **2011**, *133*, 7264−7267.

(6) Lee, Y.; Suntivich, J.; May, K. J.; Perry, E. E.; Shao-Horn, Y. Synthesis and Activities of Rutile IrO2 and RuO2 Nanoparticles for Oxygen Evolution in Acid and Alkaline Solutions. *J. Phys. Chem. Lett.* **2012**, *3*, 399−404.

(7) Gao, M. R.; Xu, Y. F.; Jiang, J.; Zheng, Y. R.; Yu, S.-H. Water Oxidation Electrocatalyzed by An Efficient $Mn_3O_4/CoSe_2$ Nanocomposite. *J. Am. Chem. Soc.* **2012**, *134*, 2930−2933.

(8) Robinson, D. M.; Go, Y. B.; Greenblatt, M.; Dismukes, G. C. Water Oxidation by λ-MnO_2: Catalysis by The Cubical Mn_4O_4 Subcluster Obtained by Delithiation of Spinel $LiMn_2O_4$. *J. Am. Chem. Soc.* **2010**, *132*, 11467−11469.

(9) Yeo, B. S.; Bell, A. T. Enhanced activity of Gold-supported Cobalt Oxide for The Electrochemical Evolution of Oxygen. *J. Am. Chem. Soc.* **2011**, *133*, 5587−5593.

(10) Jiao, F.; Frei, H. Nanostructured Cobalt Oxide Clusters in Mesoporous Silica as Efficient Oxygen-evolving Catalysts. *Angew. Chem., Int. Ed.* **2009**, *48*, 1841−1844.

(11) Wu, X.; Scott, K. $Cu_xCo_{3-x}O_4$ Nanoparticles for Oxygen Evolution in High Performance Alkaline Exchange Membrane Water Electrolysers. *J. Mater. Chem.* **2011**, *21*, 12344−12351.

(12) Lu, B.; Cao, D.; Wang, P.; Wang, G.; Gao, Y. Oxygen Evolution Reaction on Ni-substituted Co_3O_4 Nanowires Array Electrodes. *Int. J. Hydrogen Energy* **2011**, *36*, 72−78.

(13) Li, Y.; Hasin, P.; Wu, Y. $Ni_xCo_{3-x}O_4$ Nanowire Arrays for Electrocatalytic Oxygen Evolution. *Adv. Mater.* **2010**, *22*, 1926−1929.

(14) Nikolov, I.; Darkaoui, R.; Zhecheva, E.; Stoyanova, R.; Dimitrov, N.; Vitanov, T. Electrocatalytic Activity of Spinel Related Cobalties $M_xCo_{3-x}O_4$ (M = Li, Ni, Cu) in The Oxygen Evolution Reaction. *J. Electroanal. Chem.* **1997**, *429*, 157−168.

(15) Castro, E. B.; Gervasi, C. A. Electrodeposited Ni-Co-oxide Electrodes: Characterization and Kinetics of The Oxygen Evolution Reaction. *Int. J. Hydrogen Energy* **2000**, *25*, 1163−1170.

(16) Che, G.; Lakshmi, B. B.; Fisher, E. R.; Martin, C. R. Carbon Nanotubule Membranes for Electrochemical Energy Storage and Production. *Nature* **1998**, *393*, 346−349.

(17) Li, Y.; Tan, B.; Wu, Y. Ammonia-evaporation-induced Synthetic Method for Metal (Cu, Zn, Cd, Ni) Hydroxide/oxide Nanostructures. *Chem. Mater.* **2008**, *20*, 567−576.

(18) Lu, Z.; Zhu, W.; Lei, X.; Williams, G. R.; O'Hare, Z.; Chang, D. O.; Sun, X.; Duan, X. High Pseudocapacitive Cobalt Carbonate Hydroxide Films Derived From CoAl Layered Double Hydroxides. *Nanoscale* **2012**, *4*, 3640−3643.

(19) De Pauli, C. P.; Trasatti, S. Composite Materials for Electrocatalysis of O_2 Evolution: IrO_2+SnO_2 in Acid Solution. *J. Electroanal. Chem.* **2002**, *538-539*, 145−151.

(20) Morimitsu, M.; Otogawa, R.; Matsunaga, M. Effects of Cathodizing on The Morphology and Composition of IrO_2 Ta_2O_5/Ti Anodes. *Electrochim. Acta* **2000**, *46*, 401−406.

(21) Martelli, G. N.; Ornelas, R.; Faita, G. Deactivation Mechanisms of Oxygen Evolving Anodes at High Current Densities. *Electrochim. Acta* **1994**, *39*, 1551−1558.

(22) Koza, J. A.; He, Z.; Miller, A. S.; Switzer, J. A. Electrodeposition of Crystalline Co_3O_4-A Catalyst for The Oxygen Evolution Reaction. *Chem. Mater.* **2012**, *24*, 3567−3573.

(23) Nakagawa, T.; Beasley, C. A.; Murray, R. W. Efficient Electro-oxidation of Water Near Its Reversible Potential by A Mesoporous IrO_2 Nanoparticles Film. *J. Phys. Chem. C* **2009**, *113*, 12958−12961.

(24) Lyons, M. E. G.; Brandon, M. P. A Comparative Study of The Oxygen Evolution Reaction on Oxidised Nickel, Cobalt and Iron Electrodes in Base. *J. Electroanal. Chem.* **2010**, *641*, 119−130.

(25) Kinoshita, K. *Electrochemical Oxygen Technology*; John Wiley & Sons, Inc.: New York, 1992.

(26) Lyons, M. E. G.; Brandon, M. P. The Oxygen Evolution Reaction on Passive Oxide Covered Transition Metal Electrodes in Alkaline Solution. Part II—Cobalt. *Int. J. Electrochem. Sci.* **2008**, *3*, 1386−1424.

(27) Palmas, S.; Ferrara, F.; Vacca, A.; Mascia, M.; Polcaro, A. M. Behavior of Cobalt Oxide Electrodes During Oxidative Processes in Alkaline Medium. *Electrochim. Acta* **2007**, *53*, 400−406.

(28) Singh, S. P.; Samuel, S.; Tiwari, S. K.; Singh, R. N. Preparation of Thin Co_3O_4 Films on Ni and Their Electrocatalytic Surface Properties Towards Oxygen Evolution. *Int. J. Hydrogen Energy* **1996**, *21*, 171−178.

(29) King, W. J.; Tseung, A. C. C. The Reduction of Oxygen on Nickel-cobalt oOxides: The Influence of Composition and Preparation Method on The Activity of Nickel-cobalt Oxides. *Electrochim. Acta* **1974**, *19*, 485−491.

(30) Windisch, C. F.; Exarhos, G. J.; Ferris, K. F.; Engelhard, M. H.; Stewart, D. C. Infrared Transparent Spinel Films With p-type Conductivity. *Thin Solid Films* **2001**, *398-399*, 45−52.

(31) Spinolo, G.; Ardizzone, S.; Trasatti, S. Surface Characterization of Co_3O_4 Electrodes Prepared by The Sol-gel Method. *J. Electroanal. Chem.* **1997**, *423*, 49−57.

DOI: 10.1021/acsami.5b05149
ACS Appl. Mater. Interfaces 2015, 7, 21745−21750

(32) Estrada, W.; Fantini, M. C. A.; De Castro, S. C.; Polo da Fonseca, C. N.; Gorenstein, A. Radio Frequency Sputtered Cobalt Oxide Coating: Structural, Optical And Electrochemical Characterization. *J. Appl. Phys.* **1993**, *74*, 5835−5841.
(33) Bahlawane, N.; Premkumar, P. A.; Feldmann, J.; Kohse-Höinghaus, K. Preparation of Doped Spinel Cobalt Oxide Thin Films And Evaluation of Their Thermal Stability. *Chem. Vap. Deposition* **2007**, *13*, 118−122.
(34) Haenen, J.; Visscher, W.; Barendrecht, E. Characterization of $NiCo_2O_4$ Electrodes For O_2 Evolution: Part I. Electrochemical Characterization of Freshly Prepared $NiCo_2O_4$ Electrodes. *J. Electroanal. Chem. Interfacial Electrochem.* **1986**, *208*, 273−296.

DOI: 10.1021/acsami.5b05149
ACS Appl. Mater. Interfaces 2015, 7, 21745−21750